Actuators for Active Flow Control

Louis N. Cattafesta III and Mark Sheplak

Interdisciplinary Microsystems Group, Department of Mechanical and Aerospace Engineering, University of Florida, Gainesville, Florida 32611; email: cattafes@ufl.edu, sheplak@ufl.edu

Annu. Rev. Fluid Mech. 2011. 43:247–72

First published online as a Review in Advance on August 24, 2010

The *Annual Review of Fluid Mechanics* is online at fluid.annualreviews.org

This article's doi: 10.1146/annurev-fluid-122109-160634

0066-4189/11/0115-0247$20.00

Keywords

aerodynamic control, transducers, electromechanical, zero-net mass flux, fluidic, plasma

Abstract

Actuators are transducers that convert an electrical signal to a desired physical quantity. Active flow control actuators modify a flow by providing an electronically controllable disturbance. The field of active flow control has witnessed explosive growth in the variety of actuators, which is a testament to both the importance and challenges associated with actuator design. This review provides a framework for the discussion of actuator specifications, characteristics, selection, design, and classification for aeronautical applications. Actuator fundamentals are discussed, and various popular actuator types used in low-to-moderate speed flows are then described, including fluidic, moving object/surface, and plasma actuators. We attempt to highlight the strengths and inevitable drawbacks of each and highlight potential future research directions.

1. OVERVIEW

Active flow control necessarily requires actuators to interact with the flow. This field has witnessed explosive growth recently because of the ubiquitous nature of fluids in engineering systems, the community's improved understanding of fluid mechanics, and the potential to dramatically improve system performance using effective control strategies. However, the number of instances in which active flow control has successfully transitioned from a laboratory prototype to a real-world aeronautical application is small (e.g., Pugliese & Englar 1979, Kibens et al. 1999, Nagib et al. 2004, Greska et al. 2005, Seiner et al. 2005, Shaw et al. 2006). This is a testament to the difficulties associated with designing active flow control systems. This review focuses on one component specifically: actuators.

Given the interest in and importance of the topic, it is timely to assess the characteristics of the most common actuators within the context of a general design problem. Owing to space constraints, it is not possible to summarize all interesting research in this area. The primary objective is to provide a framework for assessing any flow control actuator. In an effort to achieve this, we discuss the fundamentals of actuator design and inevitable trade-offs. Dimensional analysis is used to identify key dimensionless performance metrics. Potential classifications are summarized, as different applications inevitably impose certain restrictions. Various technologies are compared to highlight their strengths and limitations. Finally, new design trends and possible future research directions are identified and discussed.

Bandwidth: range of frequencies over which the output of the actuator is deemed acceptable

Control authority: application-specific term to indicate metric of actuator performance; examples include velocity, momentum, vorticity flux, and body force

Transducer: any device that converts a signal from one energy domain to another

Feedback: process in which sensor output from a system provides information used to modify the system via a control law and an actuator

2. INTRODUCTION

2.1. Historical Perspective

Gad-el Hak (2000) and Williams & MacMynowski (2009) provide a brief history of flow control and acknowledge that the modern era began with Prandtl's early experiments on boundary layers. Generally speaking, active control implies energy addition via an actuator (MacMynowski & Williams 2009). At a minimum, the actuator can be turned on or off, and some operational characteristics can be adjusted. Active flow control varies from brute-force techniques, in which the amplitude is sufficient to modify the mean flow structure, to more efficient approaches that seek to leverage flow instabilities using small-amplitude perturbations. As our collective understanding of fluid mechanics has improved, the community has migrated toward small-amplitude forcing in which it is feasible to reduce actuator power, size, and mass, for example (Theofilis 2009). But in many cases, such as in high-speed flows, effective small-amplitude forcing remains an elusive goal because actuators generally lack sufficient bandwidth and/or control authority. These and related terms are defined and discussed in Section 3.1.

Active flow control is a multidisciplinary field with increased participation from researchers in seemingly unrelated areas. Beyond fluid mechanicians, the field has attracted researchers in fields such as applied mathematics, physics, transducers, and controls. The disparate skill sets between researchers in these fields have historically led to communication barriers that impede progress. For example, feedback flow control has gradually made inroads in the active flow control community (Rowley & Batten 2009). Beyond sensor issues, feedback control imposes additional dynamic requirements on actuators that are often ignored or underappreciated by many experimentalists with experience in open-loop control (i.e., no feedback). Conversely, theoretical control specialists often ignore the practical limitations of current hardware. Finally, transducer designers rarely consider some unique aspects of flow actuation, such as actuator placement and the physics of the fluid/actuator interaction.

2.2. Actuator Types

There are various types of actuators used in flow control applications, and these can be classified in numerous ways. One useful classification is illustrated in **Figure 1**, in which the actuators are organized based on function. The most common type is fluidic, which uses fluid injection or suction. Within this classification, there are zero-net mass-flux (ZNMF) or synthetic jet actuators (Glezer & Amitay 2002). ZNMF devices, by definition, alternately ingest and expel fluid in an oscillatory manner through an orifice/slot using only the working fluid with no external mass source/sink. Nonzero mass-flux devices, on the other hand, require a fluid source/sink and can employ steady and/or unsteady (e.g., pulsed) forcing using some combination of a valve (Seifert et al. 1993, 1996; Bachar 2001), a natural fluidic oscillator (Viets 1975), and/or combustion-driven device (Crittenden et al. 2001). They also can range in scale from conventional macroscale to submillimeter-scale microjets (Alvi et al. 2003).

Time response: a measure of the time constant of a system to a transient input, such as a step or impulse

Another class involves a moving body inside or on the domain boundary. Although fluidic devices usually involve some moving part, with the notable exception of most fluidic oscillators, their primary function is fluidic injection or suction. Alternatively, the purpose of the moving object/surface is to induce local fluid motion. An example is the electrodynamic ribbon oscillator used in the classic flat-plate experiments of Schubauer & Skramstad (1948) on laminar boundary layer transition. Other examples listed in **Figure 1** include vibrating flaps (Katz et al. 1989, Cattafesta et al. 1997, Seifert et al. 1998), time-periodic motion of a surface-mounted diaphragm (Kim et al. 2003), an oscillating wire (Bar-Sever 1989), rotating surface elements (Viets et al. 1981), and morphing surfaces (Thill et al. 2008).

The final class considered in this review is plasma actuators, which have gained popularity in recent years because of their solid-state nature and fast time response. Moreau (2007) has reviewed plasma actuators and their applications. The most popular variant is the single dielectric barrier

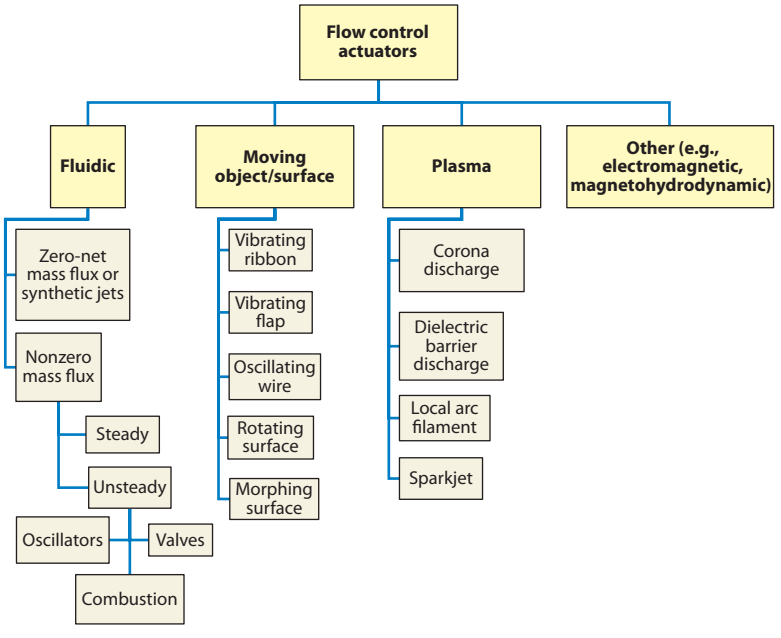

Figure 1

A type classification of flow control actuators.

discharge (SDBD) plasma actuator, which has been the subject of detailed reviews explaining the physics, design, and applications in Corke et al. (2007) and more recently in Corke et al. (2010). Other plasma devices potentially suitable for high-speed flows include local arc filament (Samimy et al. 2004) and sparkjet (Cybyk et al. 2004, Narayanaswamy et al. 2010) actuators. The devices listed in the last column of **Figure 1** are beyond the scope of this review.

Gain: the magnitude of the complex ratio of system output to input; an example is the magnitude of the frequency response of a system

Sensitivity: ratio of a sensor's electrical output to engineering input

3. ACTUATOR FUNDAMENTALS

3.1. Actuators Versus Sensors

This section summarizes important characteristics of an actuator. **Figure 2** compares the characteristics and design issues associated with actuators, which are intrusive by definition, versus sensors, which are ideally nonintrusive. First, the input and output are reversed. The input to an unsteady sensor is a flow disturbance (e.g., velocity fluctuation), and the output is an electrical quantity (e.g., voltage). For an actuator, an input electrical signal produces an output flow disturbance. So the actuator gain is essentially the inverse of sensor sensitivity. For example, the output gain of a synthetic jet can be quantified using output velocity per unit voltage [$(\mathrm{m\ s^{-1}})/V$], whereas the sensitivity of a velocity sensor is defined as the output voltage per unit velocity [$V/(\mathrm{m\ s^{-1}})$].

Although an ideal sensor only responds to the quantity of interest, it may be sensitive to other input flow variables. For example, a sensor may exhibit sensitivity to temperature, electromagnetic

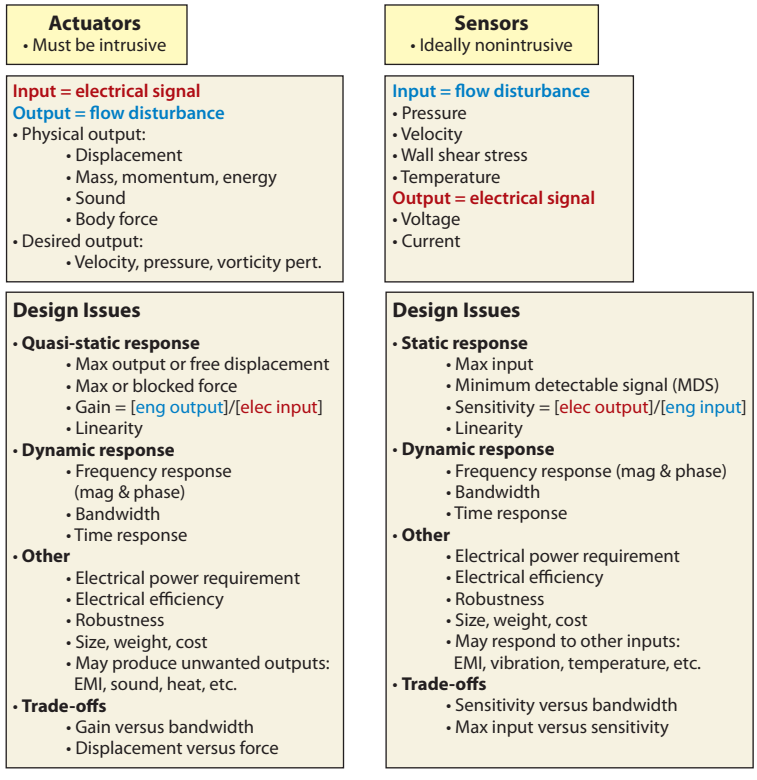

Figure 2

A comparison between actuators and sensors for flow control. Abbreviations: EMI, electromagnetic interference.

interference, or vibration, etc. An actuator, alternatively, may produce parasitic perturbations, such as electromagnetic interference, sound, or heat. A unique aspect of actuators is the actuator/fluid interaction, which dictates how the physical output of actuators, such as surface motion or momentum via fluidic injection, couples with the flow in either a linear or nonlinear manner. For example, small perturbations can excite flow instabilities, whereas large amplitudes can significantly modify the mean flow and its corresponding stability characteristics (Theofilis 2009).

Frequency response: the steady-state response of a (stable) linear system to a sinusoidal input

Many of the terms used to characterize sensors are also relevant for actuators. In terms of its static response, a sensor is specified by its maximum input level and its minimum detectable signal, and their ratio provides the dynamic range of the sensor. Similarly, the quasi-static (i.e., low-frequency) actuator response is characterized by its maximum output when the actuator is free or unloaded. At the other extreme, an actuator produces its maximum force when its direct or induced velocity is zero or blocked. Implicit in the use of any quantitative sensor is the local linear nature of the device, which is required to maintain high fidelity in spectral and correlation analysis. On the other hand, nonlinearities are often exploited in actuator design, which may increase performance at the expense of additional modeling complexity. For example, a linear electromechanical actuator (e.g., a piezo-composite vibrating beam) can be nonlinear owing to fluid/structure interaction (Cattafesta et al. 2001).

In terms of dynamic response, both sensors and actuators are characterized by frequency response (magnitude and phase) and bandwidth, but there are subtle yet important differences. The frequency response describes how the gain (for an actuator), sensitivity (for a sensor), and phase (for both) vary versus frequency for a linear system (Rowley & Batten 2009). Nonlinear actuators produce a different gain versus frequency plot for different excitation levels. Many of the fluidic actuators and moving object/surface actuators mentioned in **Figure 1** leverage a resonant phenomenon to produce a large gain at the expense of π phase shifts and nonlinear behavior. The bandwidth of an actuator refers to the range of frequencies over which the output of the device is acceptably large. This contrasts with a high-quality sensor that has a flat frequency response over the desired bandwidth of interest (e.g., a constant-temperature hot-wire anemometer).

Another often misunderstood aspect of actuator design is the importance of time response, which is the characteristic time delay to a particular input (e.g., step). The time constant and phase lag can be related in a linear system, but this is not straightforward in a nonlinear system. High-bandwidth actuators are required in active flow control systems in which the excitation frequency must be tuned to adjust to changing flow conditions. However, in feedback control systems (**Figure 3**) sensors are used to feed back (usually) random signals prevalent in turbulent flows. Assuming the sensor possesses a flat frequency response with negligible phase lag, then

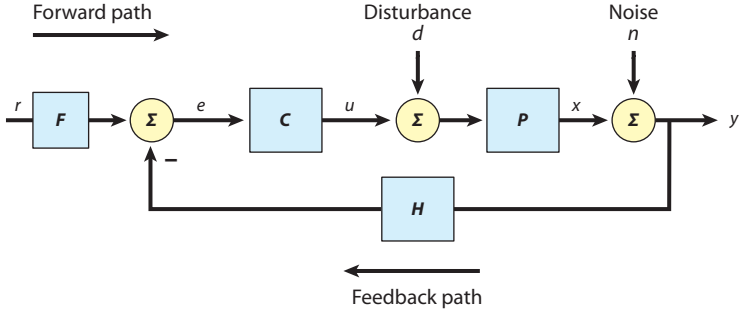

Figure 3

Schematic of a feedback control block diagram.

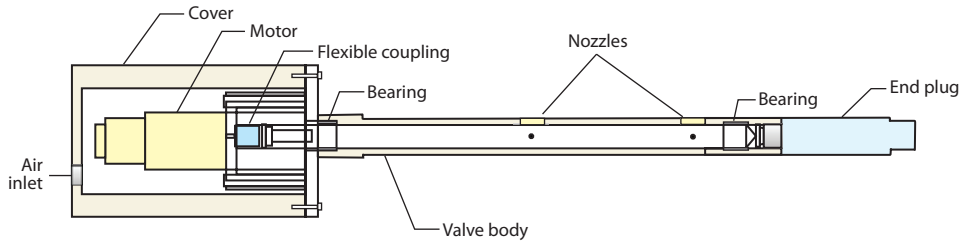

Figure 4

Schematic of a rotary valve. Figure reproduced from McManus & Magill (1996). Reprinted with permission of the American Institute of Aeronautics and Astronautics.

$H = 1$. As a result, the error signal that is fed to the controller C is random and consists of multiple frequency components, and the situation is similar for the actuator signal u. The actuator, which is part of the plant P, must be able to respond to such a complex waveform. This means that the actuator must have sufficient frequency and time response to adjust its amplitude, frequency, and phase content to track u. In other words, it must be able to provide, at any instant in time, a time-varying excitation signal containing multiple frequency components.

As an example, a rotary valve (**Figure 4**) can meet the bandwidth requirement by changing its rotational speed but, at any given time, contains only a single frequency and its harmonics due to the finite inertia of the device (McManus & Magill 1996). Similar arguments apply to standard fluidic oscillators (Viets 1975), which do not provide independent control of the amplitude and frequency and also preclude the actuator signal from phase locking to u. Counterexamples include piezoelectric- or electrodynamic-driven synthetic jets or plasmas, which can meet these requirements.

Next we consider the trade-offs inherent in actuator design. The most important actuator design characteristic is arguably its control authority or maximum gain in some cases, whereas bandwidth may be more important in other applications, such as closed-loop control (Rowley & Batten 2009). Unfortunately, these two requirements are usually at odds with each other, much like the well-known gain-bandwidth product in electronic amplifiers. For a given type, an actuator that produces higher gain has a lower bandwidth. For example, Papila et al. (2008) provide a scaling law that quantifies the trade-off between maximum volume displacement and bandwidth in the design of clamped circular piezoceramic composite diaphragms used in synthetic jets. The design goal is that the actuator should have sufficient gain over a prescribed range of frequencies, such that the actuator will have the desired control effect.

Another trade-off is generalized displacement versus generalized force. Again, the sensor analogy provides some insight. A sensor is chosen with a full-scale linear range that matches the expected maximum input. To avoid nonlinearities, the device must be stiffer than one with a smaller full-scale range and will thus possess lower sensitivity. Similarly, an actuator will provide its maximum output displacement when the load seen by the actuator is minimized, and the actuator is free. The output of an actuator often becomes nonlinear as its maximum output is approached. Alternatively, the actuator will produce its maximum force when the load is maximized and the actuator is blocked. To illustrate this trade-off, we consider the linear relation between the volume displaced ΔVol by a piezoceramic disc loaded by a differential pressure P across the diaphragm and excited by an applied voltage V_{ac}:

$$\Delta Vol = C_{aD} P + d_a V_{ac}, \tag{1}$$

where $C_{aD} = (\Delta Vol/P)_{V_{ac}=0}$ is the short-circuit acoustic compliance of the composite diaphragm and $d_a = (\Delta Vol/V_{ac})_{P=0}$ is the effective acoustic piezoelectric coefficient or the maximum gain (Prasad et al. 2006). When $P = 0$, the maximum or free displacement is $\Delta Vol_{free} = d_a V_{ac}$, where $V_{ac} = E_{\max} t_p$ is limited by the product of the coercive electric field and the piezoceramic thickness. Similarly, when $\Delta Vol = 0$, the blocked pressure is $P_{blocked} = -d_a V_{ac}/C_{aD}$. The operating point of the actuator lies along the line given by Equation 1 somewhere between these two intercepts. The design goal then is to increase ΔVol_{free} and $P_{blocked}$ subject to application-specific design constraints.

Other desirable traits include low power, high efficiency, reasonable cost, and robustness. The actuator should satisfy size and weight requirements for the specific application, and, in general, smaller size and weight are desirable. In addition, an accurate model for design, scaling, and overall control-system design is also desirable.

Seifert (2007) discusses potential dimensionless metrics. One is called the overall figure of merit:

$$OFM \equiv \frac{F_a^2 U_p}{W_a Power}, \tag{2}$$

where F_a is the thrust, U_p is the peak velocity, W_a is the weight of the actuator system, and *Power* is the power consumption. The overall figure of merit, or metrics similar to it, defines an objective function that can be used for design optimization. However, it is difficult to define a universal performance metric suitable for all actuators and applications. For example, nanosecond surface discharge plasma actuators appear to be quite effective but produce little discernible fluid velocity (Roupassov et al. 2009).

3.2. Dimensional Analysis

This section briefly addresses dimensional analysis and its relevance to flow control actuators. Dimensional analysis can be used to properly describe the effects of flow control actuators in wind-tunnel experiments and then scale the results to full-scale applications. The lack of dimensional analysis often hinders the assessment of an actuator for a potential application.

The simplified example of separation control using ZNMF actuators illustrates some of the issues. First let us consider the actuator operating in ambient conditions driven by a sinusoid with angular frequency $\omega = 2\pi f$ (Holman 2006). An assumed incompressible ZNMF actuator (**Figure 5*a***) that displaces a cavity volume ΔVol synthesizes a jet from a two-dimensional slot of height h and width/diameter d with a Reynolds number that is a function of three other dimensionless parameters:

$$Re_{U_j} = fun\left(\frac{h}{d}, \frac{\Delta Vol}{d^3}, S\right), \tag{3}$$

where U_j is a characteristic jet root-mean-square (rms) velocity (Cater & Soria 2002), and $S = \sqrt{\omega d^2/\nu}$ is the Stokes number. Note that $Re_{U_j}/S^2 = 1/St$, so only two of the three parameters are unique. As an alternative, the dimensionless stroke length (Smith & Glezer 1998) is often used instead of St, but these parameters are related (Holman 2006):

$$\frac{1}{St} = \frac{\bar{L}/d}{2\pi}. \tag{4}$$

The uncontrolled or baseline lift C_L and drag C_D coefficients of an airfoil in incompressible flow are functions of the chord Reynolds number $Re_c = \rho U_\infty c/\mu$ and angle of attack α. With ZNMF control, the lift and drag coefficients become functions of the actuator parameters, airfoil geometry, and the flow Reynolds number, which dictates the local boundary layer scales in the vicinity of

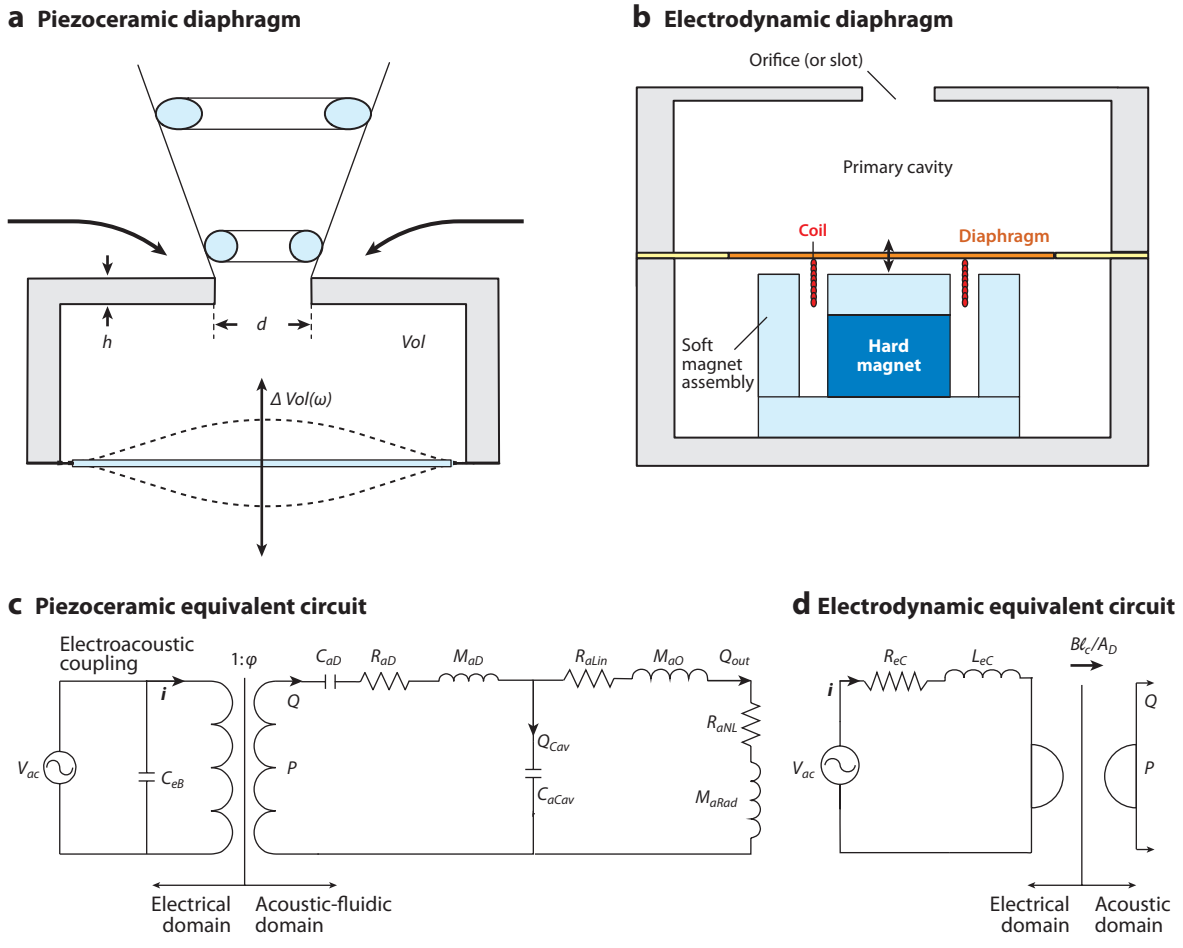

Figure 5

Schematics and equivalent circuits of the most popular versions of zero-net mass-flux (ZNMF) actuators. The right-hand side of the equivalent circuit in panel *d* (not shown) is the same as in panel *c*.

the actuator. Hence,

$$C_L = C_L\left(\frac{h}{c}, \frac{\delta^*}{c}, \frac{\delta^*}{\theta}, \frac{U_j}{U_\infty}, \frac{fc}{U_j}\right). \tag{5}$$

Experience has shown that some of the above parameters can often be combined in the form of the rms jet momentum coefficient:

$$C_\mu = \frac{\rho_j U_j^2 h}{\frac{1}{2}\rho U_\infty^2 c}. \tag{6}$$

If compressibility effects are added, either to the jet or the external flow, the list of dimensionless parameters grows. Furthermore, U_j is affected by the presence of the grazing flow (Raju et al. 2009), so C_μ, which is typically determined via measurements in quiescent conditions, is often only estimated. If the excitation signal is not sinusoidal, then additional waveform parameters become important. Finally, we note that different investigators use different velocity scales for

U_j (Smith & Glezer 1998, Cater & Soria 2002) and different length scales (e.g., the length of the separation region instead of c). All these issues and incomplete parameter specifications make it difficult to compare results. This example emphasizes the need for dimensional analysis and careful documentation of flow control experiments.

4. ACTUATOR COMPARISON

Various actuator classifications are possible. These include (*a*) open loop versus closed loop, (*b*) application, and (*c*) flow regime (i.e., low-speed, transonic). Each has its merits, but the type classification in **Figure 1** is adopted here for ease of access. **Table 1** summarizes key advantages and disadvantages of common actuators.

Table 1 Summary of common unsteady flow control actuators

Type	Subtype	Advantages	Disadvantages
Fluidic			
	ZNMF	Requires no external fluid source	Peak velocities typically limited to low to moderate subsonic speeds
		Amenable to various types of drivers and sizes	Resonant devices
		Suitable for feedback control	
	Unsteady valves	Capable of high velocities with either fast time response or high bandwidth but generally not both	May not be amenable to feedback control
			Requires an external flow source
	Oscillators	Capable of producing large disturbances	Standard versions not suitable for feedback control
		Amenable to a range of sizes and hence frequencies	Requires an external flow source
		Potential extensions possible to enable independent control of frequency and velocity	
	Combustion	Capable of producing large perturbations in high-speed flows	Currently limited to relatively low frequencies (a few hundred hertz)
			Requires combustion
Moving surface			
	Piezoelectric flaps	Simple design amenable to different frequency ranges of interest	Has constant product of max deflection and bandwidth
		Can produce spanwise or streamwise vorticity	Susceptible to fluid loading
		Suitable for feedback control	Resonant devices
	Active dimples	Potentially suitable for feedback control of turbulent wall-bounded flows	Further development needed to achieve required size and frequency response
Plasma			
	SDBD	Easily installed on models	Limited velocity output
		Low mass	Requires high voltage (kV)
		Fast time response	
		No moving parts	
	Sparkjet	All solid-state device capable of producing large perturbations in high-speed flows	Potential issues associated with EMI, acoustic level, and high temperature

Abbreviations: EMI, electromagnetic interference; SDBD, single dielectric barrier discharge; ZNMF, zero-net mass flux.

4.1. Fluidic

ZNMF or synthetic jet actuators have been reviewed by Glezer & Amitay (2002). Here, we emphasize recent developments associated with their modeling and design.

4.1.1. ZNMF actuators. **Figures 5*a*,*b*** show schematics of the standard piezoelectric and electrodynamic configurations. The diaphragm oscillates about its equilibrium position, alternately expelling/ingesting fluid from/into the cavity through an orifice or slot. In **Figure 5*a***, a piezoceramic composite diaphragm is clamped or pinned at its boundary. When excited by an ac voltage, the diaphragm bends because of the reverse piezoelectric effect and displaces a fluid volume ΔVol. In **Figure 5*b***, a diaphragm or piston is driven by a voice coil, which uses electrodynamic transduction (McCormick 2000, Nagib et al. 2004, Agashe et al. 2009). The magnet assembly generates a permanent magnetic field with magnetic flux density B, and an ac current i passing through a wound coil of length ℓ produces an ac electromagnetic force $F = B\ell i$ that causes the diaphragm to oscillate.

Other transduction schemes are possible and have their own advantages and disadvantages. For example, capacitive schemes are easily amenable to microfabrication techniques, whereas microfabricated piezoelectric and electrodynamic devices require more sophisticated approaches (Coe et al. 1994, Madou 1997). Capacitive devices are highly nonlinear for large deflections required to obtain high velocities, whereas piezoelectric and electrodynamic transducers are often adequately described by linear models. All these drivers are capable of producing multifrequency waveforms suitable for feedback control.

The primary advantages of piezoelectric transduction are low-power requirements, high bandwidth, and broadband output from dc to the several kilo-Hertz range. Electrodynamic devices are attractive for low-frequency applications because of their large displacement capability, but their increased weight (due to the magnet assembly) and heat transfer (due to heating in the resistive coil) present design challenges (McCormick 2000, Nagib et al. 2004, Agashe et al. 2009). The primary disadvantages of conventional ZNMF devices include the following: (*a*) They typically achieve a maximum velocity below approximately 100 m s^{-1}, and (*b*) they must be operated at or near resonance for satisfactory performance. Operating near mechanical resonance can lead to mechanical failure of the device (Tesar et al. 2006). In addition, 180° phase shifts associated with any resonance can lead to instability in feedback control systems (Rowley & Batten 2009). Non-negligible acoustic levels are likely at high frequencies due to the noncompact acoustic sources associated with the oscillatory fluid motion near the slot and/or the vibrating diaphragm (Devenport & Glegg 2009).

An attractive feature is that no external fluid source is required. Orifices or slots are necessarily required (and similarly for all fluidic devices) to interact with the external flow. These orifices are potentially subject to fouling. Because no external fluid source is used, any mass expelled during a cycle must be balanced by that ingested to satisfy mass conservation. From the Reynolds transport theorem, however, the net momentum flux from the orifice/slot along the jet axis during a period T is

$$\int_0^T \rho u \vec{V} \cdot \vec{n} dA > 0 \tag{7}$$

during both expulsion and ingestion. However, because of the similarity between ZNMF and conventional vortex-ring formation (Glezer 1988), researchers have historically used a characteristic jet velocity based on a slug-flow model (Smith & Glezer 1998),

$$U_0 = fL_0 = f\int_0^{T/2} u_0(t)dt, \tag{8}$$

in which U_0 is determined using only the ejection portion of the cycle from 0 to $T/2$. Cater & Soria (2002) later proposed a momentum velocity that represents a spatial- and time-averaged velocity over the entire slot area A and period

$$U_j = \left\{ \frac{1}{A} \frac{1}{T} \int_A \int_0^T [u(A,t)]^2 \, dt \, dA \right\}^{1/2}. \quad (9)$$

If the amplitude of the diaphragm motion is sufficient, one or more vortex rings are formed (Ingard & Labate 1950, Smith & Glezer 1998, Holman et al. 2005). These vortex rings synthesize a time-averaged jet due to entrainment from the surrounding fluid. Holman et al. (2005) use simple scaling and data from several sources to determine and validate a jet formation criterion, $Re_j/S^2 > K$, where K is a constant.

Substantial progress has been made in the development of low-order models of sufficient fidelity for performance prediction and design optimization (Rathnasingham & Breuer 1997, Gallas et al. 2003, Lockerby & Carpenter 2004, Prasad et al. 2006, Sharma 2007, Agashe et al. 2009, Tang & Zhong 2009). In the simplest case, lumped-element modeling (LEM) is used (Fischer 1955, Merhaut 1981, Rossi 1988). LEM provides estimates of the dynamic response of the actuator (with errors on the order of 10%). The main assumption is that the characteristic length scales of the governing physical phenomena (e.g., acoustic wavelength) are much larger than the largest dimension. When valid, the governing partial differential equations of the distributed system are lumped into a set of ordinary differential equations, and an equivalent electrical circuit is constructed using conjugate power variables (i.e., *power = effort × flow*, such as *voltage × current*, *force × velocity*, and *pressure × volume flow rate*). The lumped elements in the different energy domains are represented by their respective complex-valued impedances, $Z = effort/flow$.

For piezoelectric-driven ZNMF actuators as in **Figure 5*c***, an ac voltage V_{ac} across the composite piezoceramic diaphragm possessing a blocked electrical capacitance, C_{eB}, induces an oscillatory volume velocity by the diaphragm $Q = j\omega\Delta Vol$ and an effective pressure $P = \phi V_{ac}$, which is modeled using an electrical transformer with a turns ratio $\phi = -d_a/C_{aD}$ (see Equation 1). As the objective of the diaphragm is to displace fluid, the frequency range of interest is from dc to beyond its natural frequency but less than the second resonant frequency. The diaphragm is thus modeled by an acoustic compliance C_{aD}, the inverse of a spring constant, an acoustic damping resistance R_{aD}, and an acoustic mass M_{aD}. With the exception of R_{aD}, these lumped elements are obtained analytically using linear composite plate theory and are functions of geometry and material properties (Prasad et al. 2006).

The motion of the diaphragm either compresses/expands the fluid in the cavity or expels/ingests fluid through the orifice/slot to produce an output volume flow rate $Q_{out} = A_{out}\bar{u}$. At low frequencies, the cavity acts like a spring and is thus modeled by an acoustic compliance $C_{aCav} = Vol/(\rho c_0^2)$, where Vol is the cavity volume, and c_0 is the isentropic sound speed. Changes in fluid temperature and pressure thus affect the cavity compliance. The orifice is represented by a linear resistor R_{aLin} (i.e., major losses) and a nonlinear resistor $R_{aNL} = (K_D\, 0.5\, \rho\bar{u}^2)/Q_{out}$ (i.e., minor losses). A resistor can be added to account for acoustic radiation. The kinetic energy of the fluid in the orifice is modeled by M_{aO}, whereas the radiation mass M_{aRad} accounts for the oscillatory fluid mass or end effects. The lumped elements are analytical functions of geometry and fluid properties (with the exception of the empirical minor-loss coefficient K_D and the damping of the diaphragm R_{aD}). Equations are provided in Gallas et al. (2003) and the references therein. McCormick (2000) and Agashe et al. (2009) provide a similar framework for electrodynamic ZNMF actuators shown in **Figure 5*b***.

A key conclusion from the lumped-element analysis, which is confirmed by experiments, is that a ZNMF actuator is a coupled, nonlinear, two-degree-of-freedom oscillator with two characteristic

frequencies. One is the natural frequency of the driver $f_d = 1/\left(2\pi\sqrt{M_{aD}C_{aD}}\right)$, and the other is the Helmholtz frequency $f_H = 1/(2\pi\sqrt{(M_{aO} + M_{aRad})C_{aCav}})$ of the cavity/orifice. A common misconception is that the two resonant frequencies of the coupled oscillator, denoted as $f_1 < f_2$, are identical to f_d or f_H. But this may not be the case and, in fact, depends on the coupling between the diaphragm and the cavity. This phenomenon is discussed for linear, undamped, coupled oscillators in Fischer (1955, pp. 20–40) and Gallas et al. (2003) and can be used to an advantage when designing ZNMF actuators to obtain devices with single or dual resonant frequencies. Examples of both types are presented in Gallas et al. (2003).

There are some inherent limitations with LEM. First, the lumped assumption is valid only for devices that are sufficiently compact. Kim et al. (2005) extended the lumped-element technique to consider the relevant case of resonance and delays associated with long lengths of tubing between the driver and the orifice/slot. LEM can be extended to distributed systems using transfer matrix analysis (Chaudhry 1979, Sherman & Butler 2007). A second deficiency is that the loss parameter, $K_D \sim 1$, is an empirical constant. For steady flow, it is a function of geometry and Reynolds number. For oscillatory flow, however, as explained in Section 3.2, the list of dependent parameters expands to include the Strouhal (or Stokes) number. Lockerby & Carpenter (2004) have developed a model that solves the one-dimensional Navier-Stokes equations in the orifice, which can be incorporated in the lumped-element model. Raju et al. (2007) also incorporate additional physics into the lumped-element model using results from high-fidelity numerical simulations.

For higher-fidelity models, more sophisticated approaches short of full numerical simulations are possible (Yamaleev et al. 2005, Yamaleev & Carpenter 2006). Yamaleev et al. (2005) solve the time-dependent compressible quasi-one-dimensional Euler equations, while the diaphragm is modeled as a moving boundary. The inviscid approach satisfies conservation of mass, momentum, and energy, but it is unclear whether this approach captures the physics of the unsteady vena contracta in the orifice (Raju et al. 2007).

Rumsey et al. (2006) summarize the results of a workshop titled CFD Validation of Synthetic Jets and Turbulent Separation Control. Three test cases of varying complexity were considered by numerous contributors: (*a*) a ZNMF jet in a quiescent medium, (*b*) a ZNMF jet in a cross-flow, and (*c*) ZNMF jet control of flow over a hump model. For the isolated jet, case (*a*), several issues were noted. These included the difficulty of modeling transitional flow behavior and three-dimensional effects using Reynolds-averaged Navier-Stokes approaches. Kotapati et al. (2007) showed that it is essential to match the dimensionless jet parameters in Equation 3 using time-accurate, three-dimensional simulations via large-eddy simulation or direct numerical simulation. Despite significant simplifications in the computational fluid dynamics (CFD) model of the actuator geometry and diaphragm motion, good agreement between experiments and the simulations was obtained.

The hierarchy of modeling fidelity thus varies from a simple lumped-element model to high-fidelity numerical simulations. A CFD simulation that resolves both the small-scale details of the actuator and the large-scale behavior of the controlled flow field is impractical for routine design calculations or optimization. Alternatively, although sufficient for prediction and design purposes, LEM lacks the fidelity required to provide an appropriate time-dependent boundary condition for CFD. Thus, an important current research topic is the development of reduced-order models of a ZNMF actuator(s) suitable for use in a controlled flow field, and recent efforts in this regard are described in Raju et al. (2009).

4.1.2. Pulsed jets. Pulsed jets have been used for many years in open-loop applications with good success. It is well established that unsteady forcing has significant advantages versus steady

forcing for many flow control applications (Greenblatt & Wygnanski 2000). By definition, a steady jet has negligible temporal or ac variations. A pulsed jet is an unsteady jet that is ideally either on or off and, in the periodic case, can be characterized by a square wave with a duty cycle that indicates the percentage of time that the jet is on. Hence, pulsed jets have both a time-averaged or dc component and an unsteady or ac component. Unlike ZNMF devices, pulsed jets require an external fluid source.

A pulsed jet can be generated using, for example, a fast-acting solenoid valve (Bons et al. 2002), a high-speed rotating siren valve (Williams et al. 2007), or the rotating orifice/slot assembly like that shown in **Figure 4** (McManus & Magill 1996). A dc motor controls the rotational speed of the valve, and when the holes from the rotating inner body align with the fixed outer holes, pressurized air from the inlet is expelled. Although the bandwidth of a rotating valve may be sufficient to operate at any one of several characteristic frequencies of the flow, it is not possible to phase lock or synchronize the latter two types with a bandpass-filtered reference signal in the flow as the phase of the valve cannot be controlled. However, if the time and frequency response of the solenoid valve are sufficient, then synchronization is possible, although the type of permissible waveforms is usually restricted to variable duty-cycle square waves.

One of the primary disadvantages of a pulsed jet is the required flow source. The required average mass flow rate is usually quantified using C_μ based on the mean jet velocity and/or a dimensionless mass flow coefficient

$$C_q = \left(\rho_j U_j A_j\right) / \left(\rho_\infty U_\infty A_r\right), \tag{10}$$

where A_r is an appropriate reference area. If the mass flow rate is reduced in some manner while maintaining control authority, then the system cost of a pulsed jet may be acceptable.

One promising concept is a pulsed microjet, which is an extension of steady microjets used to control separation (Kumar & Alvi 2006), supersonic impinging jets (Alvi et al. 2003, Lou et al. 2006), high-speed jet noise (Arakeri et al. 2003), and flow-induced cavity oscillations (Zhuang et al. 2006). The idea is to reduce $\dot{m}_j$ by decreasing the orifice diameter while maintaining high jet momentum. By pulsing the jet, the mean velocity component is reduced relative to that of a steady jet, whereas the unsteady momentum coefficient based on the rms jet velocity (using Equations 6 and 9) remains large. Pulsed microjets can be obtained using the same approaches as for their macroscale counterparts. For example, Ibrahim et al. (2002) used a high-speed motor capable of achieving maximum rotational speeds of 12,000 rpm to enable unsteady forcing at 6,300 Hz of compressible jets for mixing enhancement. Choi et al. (2006) devised a scheme to pulse the microjets using a rotating-cap assembly. Although none of these actuators is suitable for closed-loop control, the following two variations are. Hogue et al. (2010) and Oates & Liu (2009) used a piezoelectric stack actuator and hydraulic amplifier circuit to produce oscillatory flow through a 400-μm-diameter microjet at frequencies up to 800 Hz. Hogue et al. (2009) also demonstrated a deformable converging-diverging micronozzle using a compact piezoelectric stack actuator that varies the nominal 1.5-Mach number by ∼25%.

Vortex generator jets are similar to microjets but have been used much more extensively (Compton & Johnston 1992, Selby et al. 1992, Khan 2000, Bons et al. 2002, Johnston & Nishi 2002, Zhang 2003, Godard & Stanislas 2006, Warsop et al. 2007). The concept is to mimic conventional vortex generators in a fluidic manner by skewing and pitching the jet axis with respect to the free-stream flow direction (see **Figure 6**). Conventional vortex generators that are always present add parasitic drag, whereas vortex generator jets can be deployed when required. An effective periodically spaced vortex-generator-jet array produces corotating streamwise vortices that stay within the boundary layer and inhibit separation via momentum exchange. Pulsing the jet reduces the required mass flow rates without jeopardizing performance benefits (Bons et al. 2002).

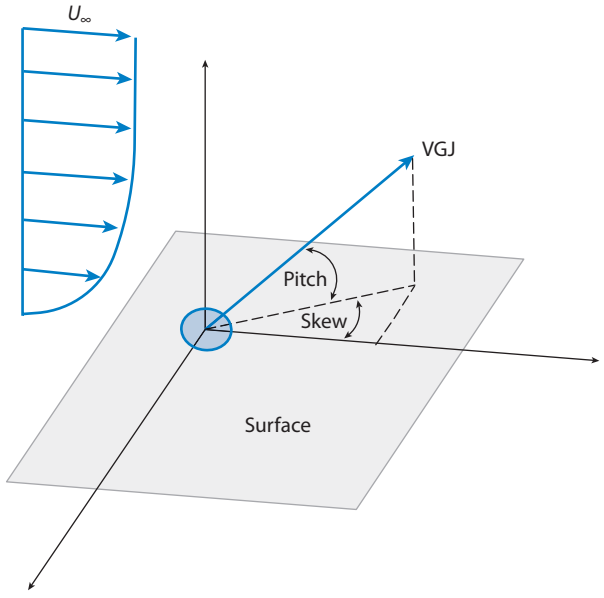

Figure 6

Schematic of a vortex generator jet (VGJ).

Warsop et al. (2007) have developed a microfabricated piezoelectric version of this device suitable for feedback control that produces exit velocities greater than 300 m s^{-1} through a 200-μm-diameter orifice at 500 Hz using only 50 mW.

4.1.3. Powered resonance tube. Pulsed-jet actuators are usually unable to force high-frequency instabilities due to bandwidth or time-response limitations. A different type of fluidic actuator with high-frequency forcing capability is the powered resonance tube, which leverages acoustic resonance. These actuators are adapted from the Hartmann tube first discovered by Hartmann & Trolle (1927) and have been subsequently adapted by several researchers for active flow control applications (Kastner & Samimy 2002; Stanek et al. 2002a,b; Raman et al. 2004; Sarpotdar et al. 2005).

The basic concept, illustrated in **Figure 7**, impinges either an underexpanded sonic jet or an ideally expanded supersonic jet from a nozzle into a closed tube of length *L*. A strong acoustic resonance, with fluctuating near-field pressure levels as high as 160 dB re 20 μPa, can be established

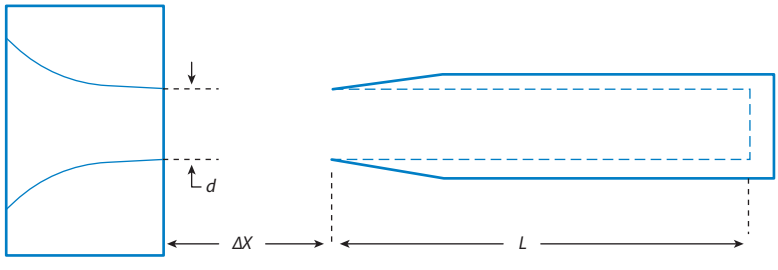

Figure 7

Schematic of a powered resonance tube.

in which incident compression waves travel down the tube and reflect from its closed end as compression waves. These waves then reflect as expansion waves at the tube entrance, which subsequently travel back down the tube length and reflect from the end as expansion waves. When these reach the tube entrance, they reflect as compression waves, and the cycle begins anew.

Raman et al. (2004) describe how a simple quarter-wave resonator model predicts the resonant frequency for long tubes, $f_r = c_0/4L$. However, the accuracy of this formula degrades for shorter tubes, and the finite reactance of the fluid mass in the gap (i.e., end effects) must be accounted for to improve the prediction (Kerschen et al. 2004). The resonant frequency can be adjusted over a wide range, from 1.6 to 15 kHz in Raman et al. (2004), by varying L. In practice, Raman et al. (2004) implemented both a look-up table and feedback control schemes to automatically adjust L and/or the gap Δx to achieve a desired resonant frequency.

The main attraction of these actuators is their ability to generate large high-frequency excitations potentially suitable for control of high-speed flows—hence the name HIFEX. Although theories have been proposed about the mechanism responsible for control (Stanek et al. 2002a,b, 2003), it is important to emphasize that these devices impart momentum to the flow and a nonzero $\dot{m}$ with $C_q \approx 1\%$ based on the cavity opening area. These disturbances thus affect not only the targeted high-frequency instabilities but also the mean flow (Ukeiley et al. 2004). Because the disturbances are large, this has two possible effects. First, the mean flow instability characteristics are modified. Second, the large disturbances may produce nonlinear interactions between multiple frequency scales.

Another point worth noting is that, although these actuators possess high bandwidth and tunable resonant frequencies, they do not have fast time response. Hence, the excitation signal frequency cannot be changed rapidly. As with rotary-valve-based devices, these actuators cannot be phase locked to a measured signal in the flow. The amplitude of the disturbances cannot be precisely controlled either. Hence, this actuator is not suitable for feedback control.

4.1.4. Combustion actuators. The combustion-driven actuator is a pulsed jet that is produced by the ignition of a mixture of gaseous fuel and oxidizer in a small (cm^3 scale) combustion chamber (Crittenden et al. 2001, Crittenden 2003, Glezer & Crittenden 2003, Cutler et al. 2005). The cycle begins with the injection of premixed fuel and oxidizer into the combustion chamber, displacing the remaining combustion products from the previous cycle. An integrated small-scale spark ignites the mixture, and a combustion process ensues that typically lasts several milliseconds (depending on the type of fuel, mixture ratio, and physical sizes of the combustor and orifice). The combustion results in a rapid pressure rise in the chamber and the ejection of a pulsed high-speed jet through one or more orifices. The operating frequency can be varied by controlling the flow rate of the fuel/oxidizer and the ignition frequency. Frequencies greater than 150 Hz have been achieved with chamber pressures of up to 5 atm, and these devices are capable of producing sonic velocities at the jet orifice. Significant jet penetration into a cross-flow at Mach numbers up to 0.7 has been demonstrated (Crittenden et al. 2001).

The primary attraction of this device is its high velocity output. However, because of the finite time duration associated with the combustion cycle, the device is limited in its current form to relatively low frequencies. In addition, although similar in many respects to a synthetic jet, this device is not a ZNMF device due to the requirement for small but nonzero reactant flow. The effects of high temperature must also be considered. Finally, it should be noted that the device is not easily amenable to feedback control applications because of its discrete pulse behavior, although the ignition can be synchronized to specific flow conditions. The frequency range of this device has been extended using a fluidic oscillator (Crittenden & Raghu 2009).

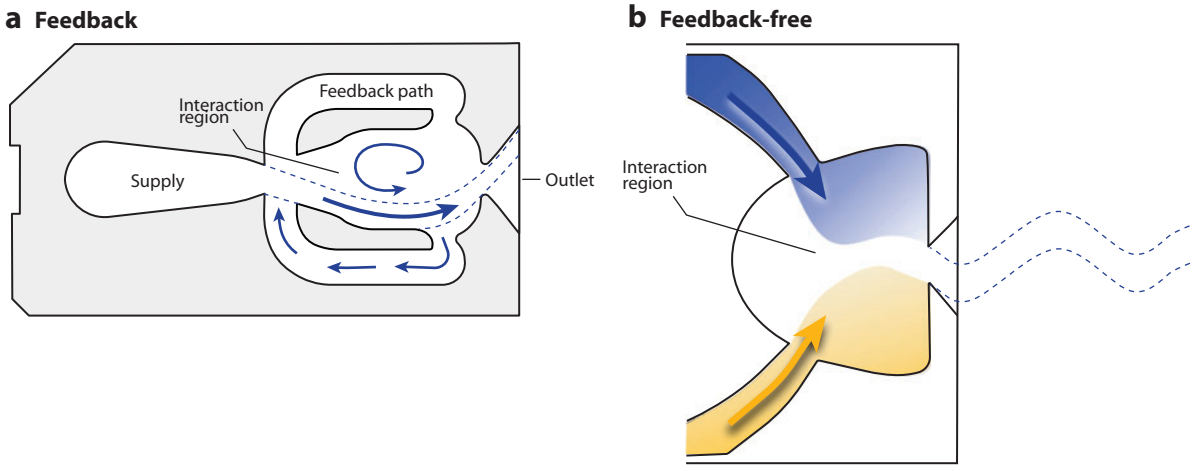

Figure 8

Schematics of two variants of fluidic actuators. Figure used with permission of Bowles Fluidics Corporation, U.S. Patents 4,463,904, 4,645,126, 4,508,267, and 6,253,782.

4.1.5. Fluidic oscillators. Fluidic oscillators are devices that generate a pulsed jet when supplied by a pressurized fluid. The standard configurations described below are potentially attractive for flow control because they have no moving parts and produce disturbances with controllable frequency. These actuators exploit fluidics technology (Kirshner 1966, Morris 1973), usually via the mechanisms of wall attachment, called the Coanda effect (Coanda 1936), and/or fluid interactions (Raghu 2001), as depicted in **Figure 8**. In the bistable fluidic nozzle shown in **Figure 8*a***, the primary flow attaches itself to either side due to the Coanda effect. The Euler-N equation, $\rho v^2/r = \partial p/\partial r$, dictates that the pressure increases in the feedback loop. This increase in pressure pushes the jet to the other side, and this process repeats in a cyclic fashion. A pulsed jet is thus obtained that sweeps from one side of the exit nozzle to the other. The flow rate of the supply jet and the length of the feedback loop are the primary parameters that establish the frequency. In **Figure 8*b***, the two jets impinge, and this leads to an unstable interaction and vortical patterns in which the jets cyclically change their position. The result is a sweeping jet pattern at the nozzle exit.

Historically, flow control applications used the subsonic flip-flop nozzle devised by Viets (1975), which was extended to supersonic speeds by Raman et al. (1993). Raman and colleagues subsequently evaluated these devices in a variety of applications (Raman & Cornelius 1995, Raman et al. 1994). Macroscale Viets devices are bulky and are typically restricted to frequencies <500 Hz. Over time, miniature integrated fluidic devices have been developed based on patented designs by Bowles Fluidics Corporation (Raghu 2001). These miniature devices have been used with good success in cavity oscillations (Raman et al. 1999), combustion control (Guyot et al. 2009), thrust vectoring (Raman et al. 2005), and separation control (Seele et al. 2009). Other promising miniature fluidic oscillators based on (*a*) the combination of an ejector and a bistable switching valve and (*b*) microimpinging jets are described in Arwatz et al. (2008) and Soloman et al. (2008), respectively.

Although the principles of operation are understood, the detailed flow physics of these actuators are not. (Interested readers are referred to a review on bifurcating jets in Reynolds et al. 2003.) Gregory and colleagues (2004, 2007b) have used a variety of diagnostic tools, including

fast-response pressure-sensitive paint, to explore the unsteady behavior of these actuators. In addition, Gokoglu et al. (2009) have used numerical simulations to shed additional light on this matter. It is important that design tools are developed for these devices that accurately predict and optimize their performance.

Although these actuators are promising, a major drawback is that the oscillation frequency is directly dependent on the flow rate through the device. It is highly desirable to decouple these two parameters. As seen in **Figure 8*a***, the feedback tubes can be eliminated and replaced with control ports. If a sufficient perturbation can be introduced at one or both of the control ports, then the jet oscillation frequency and phase can be controlled independent of the flow rate. The device is then suitable for feedback control applications. Various methods have recently been explored with mixed success, including a piezoelectric bender used as a diverter (Gregory et al. 2009), a solenoid (Culley 2006), and an SDBD actuator in one of the control ports (Gregory et al. 2007a).

4.2. Moving Object/Surface

Moving surface actuators can take various forms, but the most common are the piezoelectric composite flaps and electroactive dimples. These are summarized below.

4.2.1. Piezoelectric flaps and active dimples. The piezoelectric flap actuator has been used successfully in a variety of applications, including control of separation (Seifert et al. 1998), turbulent boundary layer streaks (Jacobson & Reynolds 1998, Jeon & Blackwelder 2000), free shear flows (Wiltse & Glezer 1993, 1998; Cattafesta et al. 2001), and flow-induced cavity oscillations (Cattafesta et al. 1997; Raman & Cain 2002; Kegerise et al. 2007a,b). A cantilever composite beam configuration is commonly used. The actuator can introduce spanwise or streamwise vortical perturbations into the flow depending on the geometry and orientation of the vibrating tip with respect to the local free-stream flow (Cattafesta & Sheplak 2009). Application of an ac voltage across the piezoceramic causes the beam to vibrate, which then interacts with the flow. Composite beam modeling is treated in Cattafesta et al. (2001) and an extension to a bimorph is presented in Mathew et al. (2006).

Typical free-tip displacements range from O(10–100 μm) for a device with a resonant frequency in excess of 1–2 kHz (Kegerise et al. 2007a) to O(1 mm) when the resonant frequency is reduced to a few hundred hertz or less. Mathew et al. (2006) describe the gain-bandwidth trade-off and design-optimization methods. A comprehensive discussion of the performance trade-offs inherent in the design and selection of microelectromechanical-systems actuators (and sensors), such as cantilevers, is presented in Bell et al. (2005). Fluid loading via two-way coupling is considered in Kudar & Carpenter (2007). Cattafesta et al. (2001) discuss a simple model for the quasi-static case when fluid loading is not significant, $f\delta/U_\infty \ll 1$.

Recent progress has been made in the microfabrication of electroactive polymer dimples for the control of turbulent boundary layers (Arthur et al. 2006, Dearing et al. 2007). A dimple consists of an elastomer sandwiched between compliant electrodes. Upon application of a voltage, an effective mechanical pressure is produced that is proportional to E_{field}^2. The induced strain in the thickness direction produces lateral expansion via the Poisson effect. The lateral strain is constrained at the boundary, which leads to out-of-plane buckling. The dimples thus produce unsteady surface depressions that interact with the near-wall turbulent structures. Research is focusing on understanding and predicting the behavior of the microfabricated dimples and ultimately designing devices with the desired size, gain, and bandwidth requirements.

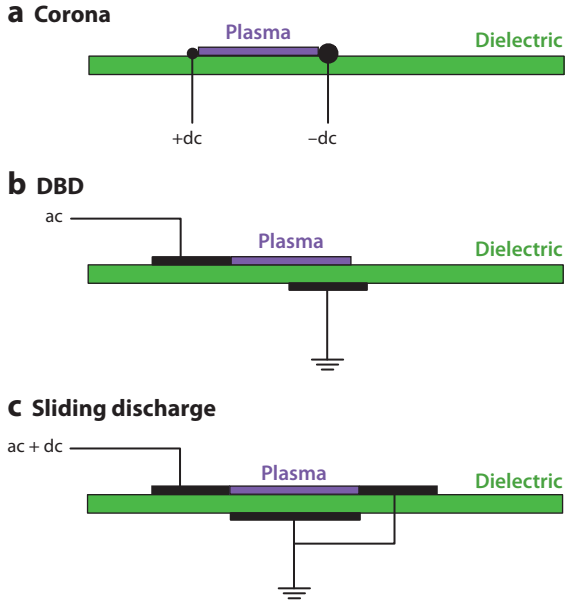

Figure 9

Schematics of three common plasma actuators: (*a*) corona, (*b*) dielectric barrier discharge (DBD), and (*c*) sliding discharge.

4.3. Plasma

SDBD actuators are becoming increasingly popular because they have no moving parts and have rapid time response and low mass, for example. The interested reader is referred to recent extensive reviews on these devices and their applications (Kunhardt 2000; Corke et al. 2007, 2010; Moreau 2007) and a dedicated edition on plasma actuators for flow control in the *Journal of Physics D: Applied Physics* (Volume 40, Number 3, February 2007). Here we focus on design-optimization trends and research issues. Some modeling approaches and issues are discussed in detail in Corke et al. (2010), Singh & Roy (2007), and Font (2006).

4.3.1. Single dielectric barrier discharge actuators. As shown in **Figure 9*b***, an SDBD actuator consists of an asymmetric pair of electrodes separated by a dielectric material. A high-voltage ac waveform, O(1–30 kV) with frequencies O(50 Hz to 20 kHz), is supplied to the exposed electrode, which results in an asymmetric electric field that ionizes air molecules to form a cold plasma in which only a small fraction of air molecules are ionized. The accelerated charged particles transfer momentum to the surrounding gas adjacent to the surface via collisions with neutral particles.

Enloe et al. (2004) provide a clear description of the plasma morphology for an SDBD actuator. In addition, they report power dissipation

$$P = \frac{1}{T}\int_0^T V_{ac}(t)\, i(t)\, dt = f\int_0^T V_{ac}(q)\, dq \tag{11}$$

by the plasma actuator for thin dielectrics as $P \propto V_{ac}^{3.5}$, whereas Pons et al. (2005) and Jolibois & Moreau (2009) show for thick dielectrics that $P \propto f(V_{ac} - V_0)^n$, where $2 < n < 3$ and V_0 is a threshold voltage. Thomas et al. (2009) describe the transition in n as the drive voltage or dielectric thickness increases.

Noting that the actuator induces a wall jet (in quiescent conditions) with a velocity profile $u(y)$, the mechanical power per unit length is

$$\frac{P_{mech}}{L} = \frac{1}{2}\int_0^\infty \rho u^3\, dy, \tag{12}$$

and the maximum efficiency is $\eta = P_{mech}/P$. The efficiency increases with dielectric thickness, but peak values on the order of only 0.1% have been observed (Jolibois & Moreau 2009).

The primary disadvantage of SDBD actuators is their diminished control authority for increasing U_∞. Hence, considerable effort has gone into maximizing the performance of SDBD actuators (Corke et al. 2010, Forte et al. 2007, Jolibois & Moreau 2009, Thomas et al. 2009). Researchers have optimized performance via parametric studies of voltage amplitude, frequency, waveform, slew rate, dielectric material and thickness, electrode geometry, multiple actuator arrays, and even the use of a plasma synthetic jet (Santhanakrishnan & Jacob 2007). A general recommendation is to use thicker dielectrics (several millimeters) with low dielectric constant for improved efficiency. Forte et al. (2007) report $U_{jet_{\max}} \approx 7$ m s^{-1} via optimization of several geometrical and electrical parameters. Likhanskii et al. (2010) provide consistent estimates of the maximum velocity under simplifying assumptions, $U_{jet_{\max}} = E_{field_{\max}}\sqrt{\varepsilon_0/\rho} \approx 8$ m s^{-1}. Boeuf et al. (2007) similarly provide estimates of the maximum body force. Jolibois & Moreau (2009) show that a physical limit is indeed reached as $U_{jet_{\max}}$ saturates at $P/L \approx 2$–3 W cm^{-1}. A unique capability of SDBD actuators is their ability to excite the flow over a wide range of time/frequency scales using unsteady actuation (Benard & Moreau 2010).

4.3.2. Other plasma actuators. Collectively, these efforts suggest that other approaches are required to significantly increase performance. Options include multiple barrier (Benard et al. 2009b, Durscher & Roy 2010) and sliding discharge actuators (Louste et al. 2005, Moreau et al. 2008, Corke et al. 2010), repetitive nanosecond-scale pulse DBD (Roupassov & Starikovskii 2008, Roupassov et al. 2009, Starikovskii et al. 2009, Unfer & Boeuf 2009), and local arc filament actuators (Samimy et al. 2004, 2007; Utkin et al. 2007). Benard et al. (2009b) describe a multiple dielectric barrier device in which the third electrode acts as a shield between two successive DBDs, resulting in a near-constant electric wind velocity above the multi-DBD actuator. A sliding discharge also uses three electrodes (**Figure 9*c***) with a combination of an ac DBD to generate a local barrier discharge and a dc component to induce the formation of extended stable plasma sheets between the two electrodes on the same side of the dielectric. An increased body force relative to the standard SDBD is produced. Short-pulse O(5–50 ns) DBD may substantially improve control authority in high-speed flows (Roupassov et al. 2009). The rapid discharge promotes rapid gas heating that creates localized shock waves with little discernible electric wind, suggesting that these are no longer cold plasmas. Localized arc filaments are similar and provide a rapid, on the order of microseconds, localized heating source capable of producing significant local pressure perturbations with independent control of the frequency and phase (Samimy et al. 2004, Utkin et al. 2007). Narayanaswamy et al. (2010) have designed a pulsed-plasma synthetic or sparkjet generated via an electrical discharge in a small cavity. Their device generates peak velocities of approximately 250 m s^{-1} at frequencies up to 5 kHz. Interested readers are referred to some additional review articles on the application of plasma to high-speed flow control and combustion (Bletzinger et al. 2005, Shang et al. 2005, Starikovskaia 2006).

Some comments on issues or potential pitfalls in SDBD actuator characterization tests are warranted. Forte et al. (2007) note that some larger seed particles used in velocity measurements may be subject to Coulomb forces, suggesting that smaller or dielectric seed particles may be required. Jolibois & Moreau (2009) point out that the maximum achievable velocity is limited by the

slew rate of the power amplifier. Thomas et al. (2009) discuss the sources of potential discrepancies between thrust-based and velocity-based measurements. Note that the induced thrust is often measured and used as an indicator of the body force, but the measured thrust is dependent on the size of the plate and includes end effects. A control volume analysis to extract $\vec{F}_{body}$ from velocity measurements on the bounding control surfaces (assuming pressure $\sim const$) may offer a consistent method for evaluation of the body force. In terms of operation in various environments, SDBD can operate at elevated relative humidity levels although with decreased efficiency (Benard et al. 2009a) and at subatmospheric pressures typical of flight conditions (Abe et al. 2008, Benard et al. 2008).

5. SUMMARY AND FUTURE TRENDS

The future is bright for active flow control, but the search for the perfect actuator continues. Of course, no such device exists due to the variety of application-specific design issues. The not-invented-here syndrome and applied nature of actuators often lead to proprietary designs and the corresponding lack of detail in publications. Unfortunately, this state of affairs impedes progress. Above we attempt to address the actuator design problem in general terms and thereby encourage researchers to think more broadly about inherent trade-offs in actuator design and how the actuator fits into the overall active flow control system.

In terms of future directions and trends, the following three areas are promising: (*a*) the development and incorporation of improved smart materials and fabrication methods, (*b*) the health monitoring of actuator performance for robust systems-level integration, and (*c*) the development of hierarchical optimized design (performance versus cost) tools. This partial list emphasizes the need for multidisciplinary collaborative efforts. A variety of modeling and design tools of varying complexity and quantifiable fidelity must be developed to assess performance over a range of conditions in applications. Based on our limited experience, we believe the flow control community must increase its emphasis on a fundamental physics-based design approach with proper recognition and disclosure of actuator limitations. This is necessary to improve the probability of successful transition of laboratory-scale devices to full-scale applications.

DISCLOSURE STATEMENT

The authors are not aware of any affiliations, memberships, funding, or financial holdings that might be perceived as affecting the objectivity of this review.

LITERATURE CITED

Abe T, Takizawa Y, Sato S, Kimura N. 2008. Experimental study for momentum transfer in a dielectric barrier discharge plasma actuator. *AIAA J.* 46:2248–56

Agashe JS, Arnold DP, Cattafesta LN. 2009. *Development of compact electrodynamic zero-net mass-flux actuators*. Presented at AIAA Aerosp. Sci. Meet., 47th, Orlando, AIAA Pap. 2009-1308

Alvi FS, Shih C, Elavarasan R, Garg G, Krothapalli A. 2003. Control of supersonic impinging jet flows using microjets. *AIAA J.* 41:1347–55

Arakeri VH, Krothapalli A, Siddavaram V, Alkislar MB, Lourenco LM. 2003. On the use of microjets to suppress turbulence in a Mach 0.9 axisymmetric jet. *J. Fluid Mech.* 490:75–98

Arthur G, McKeon BJ, Dearing S, Morrison JF, Cui Z. 2006. Manufacture of micro-sensors and actuators for flow control. *Microelectron. Eng.* 83:1205–8

Arwatz G, Fono I, Seifert A. 2008. Suction and oscillatory blowing actuator modeling and validation. *AIAA J.* 46:1107–17

Bachar T. 2001. Generating dynamically controllable oscillatory fluid flow. *U.S. Patent No. 6,186,412*
Bar-Sever A. 1989. Separation control on an airfoil by periodic forcing. *AIAA J.* 27:820–21
Bell DJ, Lu TJ, Fleck NA, Spearing SM. 2005. MEMS actuators and sensors: observations on their performance and selection for purpose. *J. Micromech. Microeng.* 15:S153–64
Benard N, Balcon N, Moreau E. 2008. Electric wind produced by a surface dielectric barrier discharge operating in air at different pressures: aeronautical control insights. *J. Phys. D Appl. Phys.* 41:042002
Benard N, Balcon N, Moreau E. 2009a. *Electric wind produced by a surface dielectric barrier discharge operating over a wide range of relative humidity*. Presented at AIAA Aerosp. Sci. Meet., 47th, Orlando, AIAA Pap. 2009-488
Benard N, Mizuno A, Moreau E. 2009b. A large-scale multiple dielectric barrier discharge actuator based on an innovative three-electrode design. *J. Phys. D Appl. Phys.* 42:235204
Benard N, Moreau E. 2010. Capabilities of dielectric barrier discharge plasma actuator for multi-frequency excitations. *J. Phys. D Appl. Phys.* 43:145201
Bletzinger P, Ganguly BN, Wie DV, Garscadden A. 2005. Plasmas in high speed aerodynamics. *J. Phys. D Appl. Phys.* 38:R33–57
Boeuf JP, Lagmich Y, Unfer T, Callegari T, Pitchford LC. 2007. Electrohydrodynamic force in dielectric barrier discharge plasma actuators. *J. Phys. D Appl. Phys.* 40:652–62
Bons JP, Rivir RB, Sondergaard R. 2002. The fluid dynamics of LPT blade separation control using pulsed jets. *J. Turbomach.* 124:77–85
Cater JE, Soria J. 2002. The evolution of round zero-net-mass-flux jets. *J. Fluid Mech.* 472:167–200
Cattafesta L, Garg S, Choudhari M, Li F. 1997. *Active control of flow-induced cavity resonance*. Presented at AIAA Fluid Dyn. Conf., 28th, Snowmass, Colo., AIAA Pap. 1997-1804
Cattafesta L, Garg S, Shukla D. 2001. Development of piezoelectric actuators for active flow control. *AIAA J.* 39:1562–68
Cattafesta L, Sheplak M. 2009. Actuators and sensors. See Joslin & Miller 2009, pp. 149–76
Chaudhry M. 1979. *Applied Hydraulic Transients*. New York: Van Nostrand Reinhold
Choi JJ, Annaswamy AM, Alvi FS, Lou H. 2006. Active control of supersonic impingement tones using steady and pulsed microjets. *Exp. Fluids* 41:841–55
Coanda H. 1936. Device for deflecting a stream of elastic fluid projected into an elastic fluid. *US Patent No. 2,052,869*
Coe D, Allen M, Trautman M, Glezer A. 1994. *Micromachined jets for manipulation of macro flows*. Presented at Solid-State Sensor Actuator Workshop
Compton DA, Johnston JP. 1992. Streamwise vortex production by pitched and skewed jets in a turbulent boundary layer. *AIAA J.* 30:640–47
Corke T, Post M, Orlov D. 2007. SDBD plasma enhanced aerodynamics: concepts, optimization and applications. *Prog. Aerosp. Sci.* 43:193–217
Corke TC, Enloe CL, Wilkinson SP. 2010. Dielectric barrier discharge plasma actuators for flow control. *Annu. Rev. Fluid Mech.* 42:505–29
Crittenden TM. 2003. *Fluidic actuators for high speed flow control*. PhD thesis. Georgia Inst. Technol., Mech. Eng.
Crittenden TM, Glezer A, Funk R, Parekh D. 2001. *Combustion-driven jet actuators for flow control*. Presented at AIAA Fluid Dyn. Conf., 31st, Anaheim, Calif., AIAA Pap. 2001-2768
Crittenden TM, Raghu S. 2009. Combustion powered actuator with integrated high frequency oscillator. *Int. J. Flow Control* 1:87–97
Culley DE. 2006. *Variable frequency diverter actuation for flow control*. Presented at AIAA Flow Control Conf., 3rd, San Francisco, AIAA Pap. 2006-3034
Cutler AD, Beck BT, Wilkes JA, Drummond JP, Alderfer DW, Danehy PM. 2005. *Development of a pulsed combustion actuator for high-speed flow control*. Presented at AIAA Aerosp. Sci. Meet. Exhib., 43rd, Reno, AIAA Pap. 2005-1084
Cybyk B, Grossman K, Wilkerson J. 2004. *Performance characteristics of the sparkjet flow control actuator*. Presented at AIAA Flow Control Conf., 2nd, Portland, AIAA Pap. 2004-2131
Dearing S, Lambert S, Morrison J. 2007. Flow control with active dimples. *Aeronaut. J.* 111:705–14
Devenport W, Glegg S. 2009. Aeroacoustics of flow control. See Joslin & Miller 2009, pp. 353–72

Durscher R, Roy S. 2010. *Novel multi-barrier plasma actuators for increased thrust*. Presented at AIAA Aerosp. Sci. Meet., Orlando, 48th, AIAA Pap. 2010-965

Enloe C, Corke T, Jumper E, Kachner K, McLaughlin T, Van Dyken R. 2004. Mechanisms and responses of a single dielectric barrier plasma actuator: plasma morphology. *AIAA J.* 42:589–94

Fischer FA. 1955. *Fundamentals of Electroacoustics*. New York: Interscience

Font G. 2006. Boundary layer control with atmospheric plasma discharges. *AIAA J.* 44:1572–78

Forte M, Jolibois J, Pons J, Moreau E, Touchard G, Cazalens M. 2007. Optimization of a dielectric barrier discharge actuator by stationary and non-stationary measurements of the induced flow velocity: application to airflow control. *Exp. Fluids* 43:917–28

Gad-el Hak M. 2000. *Flow Control: Passive, Active, and Reactive Flow Management*. Cambridge, UK: Cambridge Univ. Press

Gallas Q, Holman R, Nishida T, Carroll B, Sheplak M, Cattafesta L. 2003. Lumped element modeling of piezoelectric-driven synthetic jet actuators. *AIAA J.* 41:240–47

Glezer A. 1988. The formation of vortex rings. *Phys. Fluids* 31:3532–42

Glezer A, Amitay M. 2002. Synthetic jets. *Annu. Rev. Fluid Mech.* 34:503–29

Glezer A, Crittenden TM. 2003. Combustion-driven jet actuator. *U.S. Patent No. 6,554,607*

Godard G, Stanislas M. 2006. Control of a decelerating boundary layer. Part 3: optimization of round jets vortex generators. *Aerosp. Sci. Technol.* 10:455–64

Gokoglu SA, Kuczmarski MA, Culley DE. 2009. *Numerical studies of a fluidic diverter for flow control*. Presented at AIAA Fluid Dyn. Conf., San Antonio, 39th, AIAA Pap. 2009-4012

Greenblatt D, Wygnanski I. 2000. The control of flow separation by periodic excitation. *Prog. Aerosp. Sci.* 36:487–545

Gregory JW, Gnanamanickam EP, Sullivan JP, Raghu S. 2009. Variable-frequency fluidic oscillator driven by a piezoelectric bender. *AIAA J.* 47:2717–25

Gregory JW, Ruotolo JC, Byerley AR, McLaughlin TE. 2007a. *Switching behavior of a plasma-fluidic actuator*. Presented at AIAA Aerosp. Sci. Meet. Exhib., 45th, Reno, AIAA Pap. 2007-785

Gregory JW, Sullivan JP, Raghu S. 2004. *Visualization of internal jet mixing in a fluidic oscillator*. Presented at Int. Symp. Flow Vis., 11th, Notre Dame, Indiana

Gregory JW, Sullivan JP, Lafayette W, Raman G, Raghu S. 2007b. Characterization of the microfluidic oscillator. *AIAA J.* 45:568–76

Greska B, Krothapalli A, Seiner J, Jansen B, Ukeiley L. 2005. *The effects of microjet injection on an F404 jet engine*. Presented at AIAA/CEAS Aeroacoust. Conf., 11th, Monterey, AIAA Pap. 2005-3047

Guyot D, Paschereit CO, Raghu S. 2009. Active combustion control using a fluidic oscillator for asymmetric fuel flow modulation. *Int. J. Flow Control* 1:155–66

Hartmann J, Trolle B. 1927. A new acoustic generator. *J. Sci. Instrum.* 4:101–11

Hogue J, Brosche M, Oates W, Clark J. 2009. Development of a piezoelectric supersonic microactuator for broadband flow control. In *Proc. FCAAP: Florida Center Adv. Aero Propul. Conf., Orlando.* Tallahassee, FL: FCAAP

Hogue J, Solomon J, Hays M, Alvi F, Oates W. 2010. Broadband pulsed flow using piezoelectric microjets. *Proc. SPIE* 7643:76431V

Holman R. 2006. *An experimental investigation of flows from zero-net mass-flux actuators*. PhD thesis. Univ. Florida, Mech. Aerosp. Eng.

Holman R, Cattafesta L, Mittal R, Smith B, Utturkar Y. 2005. Formation criterion for synthetic jets. *AIAA J.* 43:2110–16

Ibrahim MK, Kunimura R, Nakamura Y. 2002. Mixing enhancement of compressible jets by using unsteady microjets as actuators. *AIAA J.* 40:681–88

Ingard U, Labate S. 1950. Acoustic circulation effects and the nonlinear impedance of orifices. *J. Acoust. Soc. Am.* 22:211–18

Jacobson SA, Reynolds WC. 1998. Active control of streamwise vortices and streaks in boundary layers. *J. Fluid Mech.* 360:179–211

Jeon WP, Blackwelder RF. 2000. Perturbations in the wall region using flush mounted piezoceramic actuators. *Exp. Fluids* 28:485–96

Johnston JP, Nishi M. 2002. Vortex generator jets: means for flow separation control. *AIAA J.* 28:989–94
Jolibois J, Moreau E. 2009. Enhancement of the electromechanical performances of a single dielectric barrier discharge actuator. *IEEE Trans. Dielectr. Electr. Insul.* 16:758–67
Joslin RD, Miller DN, eds. 2009. *Fundamentals and Applications of Modern Flow Control*. Prog. Aeronaut. Astronaut. Vol. 231. Reston, VA: AIAA
Kastner J, Samimy M. 2002. Development and characterization of Hartmann tube fluidic actuators for high-speed flow control. *AIAA J.* 40:1926–34
Katz Y, Nishri B, Wygnanski IJ. 1989. The delay of turbulent boundary layer separation by oscillatory active control. *Phys. Fluids A* 1:179–81
Kegerise M, Cabell R, Cattafesta L. 2007a. Real-time feedback control of flow-induced cavity tones, Part 1: Fixed-gain control. *J. Sound Vib.* 307:906–23
Kegerise M, Cabell R, Cattafesta L. 2007b. Real-time feedback control of flow-induced cavity tones, Part 2: Adaptive control. *J. Sound Vib.* 307:924–40
Kerschen EJ, Cain AB, Raman G. 2004. *Analytical modeling of Helmholtz resonator based powered resonance tubes*. Presented at AIAA Flow Control Conf., 2nd, Portland, AIAA Pap. 2004-2691
Khan Z. 2000. On vortex generating jets. *Int. J. Heat Fluid Flow* 21:506–11
Kibens V, Dorris J III, Smith D, Mossman M. 1999. *Active flow control technology transition—the Boeing ACE program*. Presented at AIAA Fluid Dyn. Conf., 30th, Norfolk, AIAA Pap. 1999-3507
Kim BH, Acharya M, Emo S, Williams D. 2005. Modeling pulsed-blowing systems for flow control. *AIAA J.* 43:314–25
Kim C, Jeon W-P, Park J, Choi H. 2003. Effect of a localized time-periodic wall motion on a turbulent boundary layer flow. *Phys. Fluids* 15:265–68
Kirshner JM, ed. 1966. *Fluid Amplifiers*. New York: McGraw-Hill
Kotapati RB, Mittal R, Cattafesta L. 2007. Numerical study of a transitional synthetic jet in quiescent external flow. *J. Fluid Mech.* 581:287–321
Kudar KL, Carpenter PW. 2007. Numerical investigation and feasibility study of a PZT-driven micro-valve pulsed-jet actuator. *Flow Turbul. Combust.* 78:223–54
Kumar V, Alvi FS. 2006. Use of high-speed microjets for active separation control in diffusers. *AIAA J.* 44:273–81
Kunhardt E. 2000. Generation of large-volume, atmospheric-pressure, nonequilibrium plasmas. *IEEE Trans. Plasma Sci.* 28:189–200
Likhanskii AV, Shneider MN, Opaits DF, Miles RB, Macheret SO. 2010. *Limitations of the DBD effects on the external flow*. Presented at AIAA Aerosp. Sci. Meet., 48th, Orlando, AIAA Pap. 2010-470
Lockerby DA, Carpenter PW. 2004. Modeling and design of microjet actuators. *AIAA J.* 42:220–27
Lou H, Alvi FS, Shih C. 2006. Active and passive control of supersonic impinging jets. *AIAA J.* 44:58–66
Louste C, Artana G, Moreau E, Touchard G. 2005. Sliding discharge in air at atmospheric pressure: electrical properties. *J. Electrost.* 63:615–20
MacMynowski DG, Williams DR. 2009. Flow control terminology. See Joslin & Miller 2009, pp. 59–72
Madou MJ. 1997. *Fundamentals of Micromachining*. New York: CRC
Mathew J, Song Q, Sankar B, Sheplak M, Cattafesta L. 2006. Optimized design of piezoelectric flap actuators for active flow control. *AIAA J.* 44:2919–28
McCormick DC. 2000. *Boundary layer separation control with directed synthetic jets*. Presented at Aerosp. Sci. Meet. Exhib., 38th, Reno, AIAA Pap. 2000-0519
McManus K, Magill J. 1996. *Separation control in incompressible and compressible flows using pulsed jets*. Presented at AIAA Fluid Dyn. Conf., 27th, New Orleans, AIAA Pap. 1996-1948
Merhaut J. 1981. *Theory of Electroacoustics*. New York: McGraw-Hill
Moreau E. 2007. Airflow control by non-thermal plasma actuators. *J. Phys. D Appl. Phys.* 40:605–36
Moreau E, Sosa R, Artana G. 2008. Electric wind produced by surface plasma actuators: a new dielectric barrier discharge based on a three-electrode geometry. *J. Phys. D Appl. Phys.* 41:115204
Morris NM. 1973. *An Introduction to Fluid Logic*. London: McGraw-Hill
Nagib H, Kiedaisch J, Wygnanski I, Stalker A, Wood T, McVeigh M. 2004. First-in-flight full-scale application of active flow control: the XV-15 tiltrotor download reduction. *Tech. Rep.*, Ill. Inst. Technol.

Narayanaswamy V, Raja LL, Clemens NT. 2010. Characterization of a high-frequency pulsed-plasma jet actuator for supersonic flow control. *AIAA J.* 48:297–305

Oates WS, Liu F. 2009. Piezohydraulic actuator development for microjet flow control. *ASME J. Mech. Des.* 131:14–18

Papila M, Sheplak M, Cattafesta L. 2008. Optimization of clamped circular piezoelectric composite actuators. *Sens. Actuators A Phys.* 147:310–23

Pons J, Moreau E, Touchard G. 2005. Asymmetric surface dielectric barrier discharge in air at atmospheric pressure: electrical properties and induced airflow characteristics. *J. Phys. D Appl. Phys.* 38:3635–42

Prasad SAN, Gallas Q, Horowitz S, Homeijer B, Sankar BV, et al. 2006. An analytical electroacoustic model of a piezoelectric composite circular plate. *AIAA J.* 44:2311–18

Pugliese AJ, Englar RJ. 1979. *Flight testing the circulation control wing*. Presented at Aircr. Syst. Technol. Meet., New York, AIAA Pap. 1979-1791

Raghu S. 2001. Feedback-free fluidic oscillator and method. *U.S. Patent No. 6,253,782*

Raju R, Aram E, Mittal R, Cattafesta L. 2009. Simple models of zero-net mass-flux jets for flow control simulations. *Int. J. Flow Control* 1:179–97

Raju R, Gallas Q, Mittal R, Cattafesta L. 2007. Scaling of pressure drop for oscillatory flow through a slot. *Phys. Fluids* 19:078107

Raman G, Cain AB. 2002. Innovative actuators for active flow and noise control. *Proc. Inst. Mech. Eng. G. J. Aerosp. Eng.* 216:303–24

Raman G, Cornelius D. 1995. Jet mixing control using excitation from miniature oscillating jets. *AIAA J.* 33:365–68

Raman G, Hailye M, Rice E. 1993. Flip-flop jet nozzle extended to supersonic flows. *AIAA J.* 31:1028–35

Raman G, Khanafseh S, Cain AB, Kerchen E. 2004. Development of high bandwidth powered resonance tube actuators with feedback control. *J. Sound Vib.* 269:1031–62

Raman G, Packiarajan S, Papadopoulos G, Weissman C, Raghu S. 2005. Jet thrust vectoring using a miniature fluidic oscillator. *Aeronaut. J. R. Aeronaut. Soc.* 109:129–38

Raman G, Raghu S, Bencic T. 1999. *Cavity resonance suppression using miniature fluidic oscillators*. Presented at AIAA Aeroacoust. Conf., 5th, Seattle, AIAA Pap. 1999-1900

Raman G, Rice EJ, Cornelius DM. 1994. Evaluation of flip-flop jet nozzles for use as practical excitation devices. *J. Fluids Eng.* 116:508–15

Rathnasingham R, Breuer KS. 1997. Coupled fluid-structural characteristics of actuators for flow control. *AIAA J.* 35:832–37

Reynolds WC, Parekh DE, Juvet PJD, Lee MJD. 2003. Bifurcating and blooming jets. *Annu. Rev. Fluid Mech.* 35:295–315

Rossi M. 1988. *Acoustics and Electroacoustics*. Norwood, MA: Artech House

Roupassov DV, Nikipelov AA, Nudnova MM, Starikovskii AY. 2009. Flow separation control by plasma actuator with nanosecond pulsed-periodic discharge. *AIAA J.* 47:168–85

Roupassov DV, Starikovskii AY. 2008. Development of nanosecond surface discharge in actuator geometry. *IEEE Trans. Plasma Sci.* 36:1312–13

Rowley CW, Batten BA. 2009. Dynamic and closed-loop control. See Joslin & Miller 2009, pp. 115–48

Rumsey C, Gatski T, Sellers W, Vatsa V, Viken S. 2006. Summary of the 2004 Computational Fluid Dynamics Validation Workshop on synthetic jets. *AIAA J.* 44:194–207

Samimy M, Adamovich L, Webb B, Kastner J, Hileman J, et al. 2004. Development and characterization of plasma actuators for high-speed jet control. *Exp. Fluids* 37:577–88

Samimy M, Kim JH, Kastner J, Adamovich I, Utkin Y. 2007. Active control of high-speed and high-Reynolds-number jets using plasma actuators. *J. Fluid Mech.* 578:305–30

Santhanakrishnan A, Jacob JD. 2007. Flow control with plasma synthetic jet actuators. *J. Phys. D Appl. Phys.* 40:637–51

Sarpotdar S, Raman G, Cain AB. 2005. Powered resonance tubes: resonance characteristics and actuation signal directivity. *Exp. Fluids* 39:1084–95

Schubauer GB, Skramstad HK. 1948. Laminar-boundary-layer oscillations and transition on a flat plate. *Tech. Rep. 909*, NACA

Seele R, Tewes P, Woszidlo R, McVeigh MA, Lucas NJ, Wygnanski IJ. 2009. Discrete sweeping jets as tools for improving the performance of the V-22. *J. Aircr.* 46:2098–106
Seifert A. 2007. Closed-loop active flow control systems: actuators. In *Active Flow Control*, ed. R King, pp. 85–102. Notes Numer. Fluid Mech. Multidiscip. Des. Vol. 95. Berlin: Springer
Seifert A, Bachar T, Koss D, Shepshelovich M, Wygnanskil I. 1993. Oscillatory blowing: a tool to delay boundary-layer separation. *AIAA J.* 31:2052–60
Seifert A, Darabi A, Wygnanski IJ. 1996. Delay of airfoil stall by periodic excitation. *J. Aircr.* 33:691–98
Seifert A, Eliahu S, Greenblatt D, Wygnanski IJ. 1998. Use of piezoelectric actuators for airfoil separation control. *AIAA J.* 36:1535–37
Seiner J, Ukeiley L, Jansen B. 2005. *Aero-performance efficient noise reduction for the F404-400 engine*. Presented at AIAA/CEAS Aeroacoust. Conf., 11th, Monterey, AIAA Pap. 2005-3048
Selby GV, Lin JC, Howard FG. 1992. Control of low-speed turbulent separated flow using jet vortex generators. *Exp. Fluids* 12:394–400
Shang J, Surzhikov S, Kimmel R, Gaitonde D, Menart J, Hayes J. 2005. Mechanisms of plasma actuators for hypersonic flow control. *Prog. Aerosp. Sci.* 41:642–68
Sharma RN. 2007. Fluid-dynamics-based analytical model for synthetic jet actuation. *AIAA J.* 45:1841–47
Shaw LL, Smith BR, Saddoughi S. 2006. *Full-scale flight demonstration of active control of a pod wake*. Presented at AIAA Flow Control Conf., 3rd, San Francisco, AIAA Pap. 2006-3185
Sherman C, Butler J. 2007. *Transducers and Arrays for Underwater Sound*. New York: Springer
Singh KP, Roy S. 2007. Modeling plasma actuators with air chemistry for effective flow control. *J. Appl. Phys.* 101:123308
Smith B, Glezer A. 1998. The formation and evolution of synthetic jets. *Phys. Fluids* 10:2281–97
Soloman JT, Kumar R, Alvi FS. 2008. Development and characterization of high bandwidth micro-actuator. *Proc. FEDSM2008: 2008 ASME Fluids Eng. Div. Summer Conf., Jacksonville, Florida*, FEDSM2008-55032. New York: ASME
Stanek MJ, Raman G, Ross JA, Odedra J, Peto J, et al. 2002a. *High frequency acoustic suppression—the role of mass flow, the notion of superposition, and the role of inviscid instability—a new model* (*Part II*). Presented at AIAA/CEAS Aeroacoust. Conf. Exhib., 8th, Breckenridge, CO, AIAA Pap. 2002-2404
Stanek MJ, Raman G, Ross JA, Odedra J, Peto J, et al. 2003. *High frequency acoustic suppression—the mystery of the rod-in-crossflow revealed*. Presented at Aerosp. Sci. Meet. Exhib., 41st, Reno, AIAA Pap. 2003-0007
Stanek MJ, Sinha R, Seiner J, Pierce B, Jones M. 2002b. *High frequency flow control—suppression of aero-optics in tactical directed energy beam propagation and the birth of a new model* (*Part I*). Presented at AIAA/CEAS Aeroacoust. Conf., 8th, Breckenridge, CO, AIAA Pap. 2002-2272
Starikovskaia SM. 2006. Plasma assisted ignition and combustion. *J. Phys. D Appl. Phys.* 39:R265–99
Starikovskii AY, Nikipelov AA, Nudnova MM, Roupassov DV. 2009. SDBD plasma actuator with nanosecond pulse-periodic discharge. *Plasma Sources Sci. Technol.* 18:034015
Tang H, Zhong S. 2009. Lumped element modelling of synthetic jet actuators. *Aerosp. Sci. Technol.* 13:331–39
Tesar V, Hung C, Zimmerman W. 2006. No-moving-part hybrid-synthetic jet actuator. *Sensors Actuators A Phys.* 125:159–69
Theofilis V. 2009. Role of instability theory in flow control. See Joslin & Miller 2009, pp. 73–114
Thill C, Etches J, Bond I, Potter K, Weaver P. 2008. Morphing skins. *Aeronaut. J.* 112:117–39
Thomas FO, Corke TC, Iqbal M, Kozlov A, Schatzman D. 2009. Optimization of dielectric barrier discharge plasma actuators for active aerodynamic flow control. *AIAA J.* 47:2169–78
Ukeiley LS, Ponton MK, Seiner JS, Jansen B. 2004. Suppression of pressure loads in cavity flows. *AIAA J.* 42:70–79
Unfer T, Boeuf JP. 2009. Modelling of a nanosecond surface discharge actuator. *J. Phys. D Appl. Phys.* 42:194017
Utkin YG, Keshav S, Kim JH, Kastner J, Adamovich IV, Samimy M. 2007. Development and use of localized arc filament plasma actuators for high-speed flow control. *J. Phys. D Appl. Phys.* 40:685–94
Viets H. 1975. Flip-flop jet nozzle. *AIAA J.* 13:1375–79
Viets H, Piatt M, Ball M. 1981. Boundary layer control by unsteady vortex generation. *J. Wind Eng. Ind. Aerodyn.* 7:135–44

Warsop C, Hucker M, Press AJ, Dawson P. 2007. Pulsed air-jet actuators for flow separation control. *Flow Turbul. Combust.* 78:255–81

Williams D, Cornelius D, Rowley CW. 2007. Supersonic cavity response to open-loop forcing. In *Active Flow Control*, ed. R King, pp. 230–43. Notes Numer. Fluid Mech. Multidiscip. Des. Vol. 95. Berlin: Springer

Williams DR, MacMynowski DG. 2009. Brief history of flow control. See Joslin & Miller 2009, pp. 1–20

Wiltse JM, Glezer A. 1993. Manipulation of free shear flows using piezoelectric actuators. *J. Fluid Mech.* 249:261–85

Wiltse JM, Glezer A. 1998. Direct excitation of small-scale motions in free shear flows. *Phys. Fluids* 10:2026–36

Yamaleev N, Carpenter M. 2006. Quasi-one-dimensional model for realistic three-dimensional synthetic jet actuators. *AIAA J.* 44:208–16

Yamaleev NK, Carpenter MH, Ferguson F. 2005. Reduced-order model for efficient simulation of synthetic jet actuators. *AIAA J.* 43:357–69

Zhang X. 2003. The evolution of co-rotating vortices in a canonical boundary layer with inclined jets. *Phys. Fluids* 15:3693–702

Zhuang N, Alvi FS, Alkislar MB, Shih C. 2006. Supersonic cavity flows and their control. *AIAA J.* 44:2118–28

RELATED RESOURCES

Choi H, Jeon W-P, Kim J. 2008. Control of flow over a bluff body. *Annu. Rev. Fluid Mech.* 40:113–39

Dowling AP, Morgans AS. 2005. Feedback control of combustion oscillations. *Annu. Rev. Fluid Mech.* 37:151–82

Joslin RD. 1998. Aircraft laminar flow control. *Annu. Rev. Fluid Mech.* 30:1–29

Kasagi N, Suzuki Y, Fukagata K. 2009. Microelectromechanical systems–based feedback control of turbulence for skin friction reduction. *Annu. Rev. Fluid Mech.* 41:231–51

Rowley CW, Williams DR. 2006. Dynamics and control of high-Reynolds-number flow over open cavities. *Annu. Rev. Fluid Mech.* 38:251–76

Paduano JD, Greitzer EM, Epstein AH. 2001. Compression system stability and active control. *Annu. Rev. Fluid Mech.* 33:491–517

Annual Review of
Fluid Mechanics

Volume 43, 2011

Contents

Indexes

Errata

An online log of corrections to *Annual Review of Fluid Mechanics* articles may be found at http://fluid.annualreviews.org/errata.shtml